PCCP

PAPER

View Article Online
View Journal | View Issue

Cite this: *Phys. Chem. Chem. Phys.*, 2025, **27**, 16161

Coupling and decoupling of molecular reorientation and charge transport in Li-salt-doped cycloalcohol ion conductors†

Sofiane Lansab, [a] Yannik Hinz, [a] Bastian Grabe, [b] Peter Lunkenheimer [c] and Roland Böhmer [a]

Received 27th May 2025,
Accepted 25th June 2025

DOI: 10.1039/d5cp02003d

rsc.li/pccp

Using broadband impedance spectroscopy and conductometry, we study the phase behavior and the reorientational and translational dynamics of cycloalcohols doped with 1 to 20 mol% of Li salt. At low salt concentrations, a plastically crystalline state is stable. In this regime, the dielectric spectra of the cycloalcohols reveal two relaxation processes. One of them originates from the α-relaxation and indicates an orientational glass transition. The other, much slower process, is related to ionic hopping. By comparing reorientation times with electrical conductivities, for 1 mol% Li doping, previous studies suggested an only weak decoupling of rotational and translational motions. Rather than analyzing disparate quantities, the present work directly compares peak frequencies corresponding to reorientational and translational rates. This approach allows one to resolve the mild, yet significant divergence of the two rates, *i.e.*, a dynamic decoupling, also for higher doping levels and for different Li salts. The electrolytes that form at Li salt concentrations of 5 mol% and more display a qualitatively different behavior. In this compositional regime, a liquid-to-glass transition arises and the ion hopping time that we probe using lithium nuclear magnetic resonance and proton-detected diffusometry is compatible with the reorientational time scales. This observation implies a close coupling of both underlying degrees of freedom.

1. Introduction

The quest for batteries with solid or solid-like electrolytes drives intensive research across a host of different materials, including polymer- and ionic-liquid-based electrolytes,[1–5] superionic crystals,[6] and not the least in the field of plastic crystalline solids (PCs).[7,8] Here, molecules or molecular ions are placed on a well-defined center-of-mass lattice where they can perform fast reorientational motions. Therefore, the mobile species experience a kind of liquid-like environment. With a rotation-translation coupling present in various PCs, the fast reorientational motion in such crystals is a good candidate to enable efficient translational mobility as well. Often, the so-called "paddle-wheel" or "revolving-door" mechanism is found to facilitate the motion of intrinsic charge carriers as well as that of intentionally added ions.[9]

Among the rotator crystals that hold promise for energy storage applications are (i) molecular PCs that are doped with suitable salts[10–12] or (ii) ionic PCs,[13–17] *i.e.*, solid solutions composed of cationic and anionic constituents. In the ionic PCs, one or both of the constituents can sustain fast reorientational motions. For these electrolytes, the large charge number density and the consequent presence of strong Coulombic interactions require dedicated strategies so that an efficient ionic transport still arises. To fine-tune the overall strength of the Coulombic interactions, it can be advantageous to resort to molecular PCs (composed of uncharged species) and to dope them with an optimum amount of salt. A particularly promising approach is to combine the ideas behind scenarios (i) and (ii), so that one arrives at ionic PCs with additional salt dopants. In some examples, the plastic phase can thus be maintained to even roughly 10 mol% of added salt.[18–21]

Nevertheless, many studies focus on the doping range of only a few percent of salt, sometimes in conjunction with blending in a second, structurally related plastic crystal. In this context, Li doped mixed dinitrile-,[22–24] cycloalcohol-,[25] pyrrolidinium-,[26] and adamantane-based[27] and other[28] PCs were exploited to achieve further enhanced conductivity. Several of these mixtures were investigated using dielectric spectroscopy with the goal to sense the reorientational dynamics and using conductivity spectroscopy which probes the charge dynamics.[24,25,27] The latter method provides access to transport quantities from which, in

[a] *Fakultät Physik, Technische Universität Dortmund, D-44221 Dortmund, Germany*
[b] *Fakultät für Chemie und Chemische Biologie, Technische Universität Dortmund, D-44221 Dortmund, Germany*
[c] *Experimental Physics V, Center for Electronic Correlations and Magnetism, University of Augsburg, 86159 Augsburg, Germany*

† Electronic supplementary information (ESI) available. See DOI: https://doi.org/10.1039/d5cp02003d

favorable cases, the often sought translational correlation times can be inferred. In this vein, the increased defect density that was reported to occur in Li doped adamantane-based PCs was conjectured to govern their electrical conductivity.[27] Conversely, the paddle-wheel mechanism was directly demonstrated to be operative in Li doped dinitrile mixtures.[29] This became possible by complementing dielectric spectroscopy by using nuclear magnetic resonance (NMR) techniques. The time scales describing the molecular reorientation of the different constituents within various dinitrile mixtures were accessed using protons, deuterons, and carbons as nuclear probes; the time scales that refer to the translational cationic motions were directly determined by means of ^{7}Li NMR.[29,30]

The aforementioned dinitrile-, adamantane-, cycloalcohol-, and pyrrolidinium-based crystal alloys are miscible over the full compositional range. This situation is advantageous when studying the impact of effects related to the internal volume that is available to the charge carriers on the coupling of the orientational and translational degrees of freedom. However, it turned out that using the same type and concentration of (1 mol% $LiPF_6$) doping, the mixed crystals formed by cyclohexanol (HEX) and cyclooctanol (OCT) display much higher conductivities than the adamantane-based rotator phases.[25,27] This finding renders the $HEX_{1-x}OCT_x$ matrix, to which Li salt is added, particularly attractive for study.

For different OCT concentrations x, this salt-doped molecular plastic crystal system displays similar dynamical behaviors. Particularly for $(HEX_{0.6}OCT_{0.4})_{0.99}(LiPF_6)_{0.01}$, significant, yet relatively mild deviations from rotation-translation coupling were reported.[25] Assuming that the situation remains similar when doping with other Li-salts such as lithium bis(trifluoromethylsulfonyl)imide (LiTFSI), we chose $HEX_{0.6}OCT_{0.4}$ as a starting point for the present study. Our initial goal was to explore whether an increased Li doping to about 10 mol% and beyond would lead to a conductivity enhancement, similar to observations reported for various non-crystalline electrolytes.[21,31,32]

To anticipate some of our results, for mole fractions $c \geq 5$ mol% of Li salt, it turned out that unlike, *e.g.*, for the dinitrile-based alloys, the rotator phase of the cycloalcohol host matrix is less stable than the liquid phase. Thus, we find that at $c \geq 5$ mol% of LiTFSI, crystallization is suppressed and liquid-to-glass transitions emerge when the sample approaches low temperatures. This situation resembles that of deep eutectic solvents. Typically, such solvents are formed when a molecular (usually hydrogen-bond sustaining) constituent and an ionic species such as LiTFSI are mixed over wide compositional ranges.[21,31,33]

Previously, HEX and OCT were studied as neat crystals using various techniques involving dielectric spectroscopy,[34–36] NMR spectroscopy,[37–40] and neutron scattering.[41,42] Some cycloalcohols were also studied in salt-doped form, but as far as we know only up to the 1% level.[27] To gain insights into the interplay of plastically crystalline and supercooled liquid phases, we aim at finding out whether or not, at higher doping levels, $HEX_{1-c}LiTFSI_c$ and $OCT_{1-c}LiTFSI_c$ may show deep-eutectic-like behavior. Therefore, by examining samples with salt concentrations as large as $c = 20$ mol%, a major objective of the present work is to explore the dynamic coupling, or decoupling, of the various degrees of freedom. To reach this goal, the different NMR techniques that we exploit play an important role.

After briefly presenting the experimental details, in Section 3, we focus on the regime of weak ($c \leq 3$ mol%) Li doping in which plastically crystalline low-temperature phases are stable. Subsequently, stronger Li-doped, deep-eutectic-like glass formers are studied where the ions are dissolved in pure and in mixed cycloalcohol matrices. The interplay of the reorientational dynamics and translational mobility as probed by conductivity measurements is the focus of Section 4. Finally, we discuss the present results in the context of other electrolytes, before summarizing our findings in Section 5.

2. Experimental details

Protonated HEX, protonated OCT, LiTFSI salt (all with a purity of 99%), as well as C–D deuterated cyclohexanol (HEX-d_{11}, degree of deuteration 98%) were purchased from Sigma-Aldrich (while deuterated OCT is apparently commercially not available). Upon cooling, HEX and OCT solidify near 270 and 280 K, respectively,[25] so that at room temperature also their mixtures are liquid. The preparation of the salt doped samples with LiTFSI fractions $c = 1$, 3, 5, 8, 10, 15, and 20 mol% closely followed the procedure described in detail for other solutions that form PCs[29] or deep eutectic solvents.[31] Dielectric and conductivity experiments were carried out using a Novocontrol system. The samples were placed in a parallel-plate invar-sapphire capacitor[43] that features an electrode gap of 50 μm. Typically, ac voltages of 1 V_{rms} were applied during the frequency sweeps. With a focus on the spectral shape, the dielectric function is usually given after normalization by the high-frequency dielectric constant, ε_∞. Like in ref. 29, ^{2}H and ^{7}Li NMR relaxometry was applied using home-built spectrometers that were operated at Larmor frequencies of 46.5 and 116.9 MHz, respectively. Details of the proton-detected diffusion measurements are given elsewhere.[29]

3. Results and analyses

Weak Li doping: plastic-crystal regime

Fig. 1 shows frequency-dependent dielectric and conductivity results for $(HEX_{0.6}OCT_{0.4})_{0.97}(LiTFSI)_{0.03}$. Frame (a) displays the real part ε' of the complex dielectric constant $\varepsilon^* = \varepsilon' - i\varepsilon''$ from which a clear double step is seen. Such a somewhat uncommon behavior was previously reported for Li-doped adamantane-based crystals.[27] Faint indications for such a feature were noted for dinitriles devoid of added salt.[44] For $(HEX_{0.6}OCT_{0.4})_{0.99}(LiPF_6)_{0.01}$, *i.e.*, for a PC with a different OCT concentration, some hints of a second low-frequency relaxation step are noted in ref. 25, but not analyzed in any detail.

For $(HEX_{0.6}OCT_{0.4})_{0.97}(LiTFSI)_{0.03}$, the Li salt generates strong electrical conductivity, which overlays any dielectric loss peaks. Fig. 1(b) shows an example for $T = 233$ K. The derivative[45,46]

$$\varepsilon''_{der}(2\pi\nu) \equiv -\frac{\pi}{2}\frac{d\varepsilon'(2\pi\nu)}{d\ln(2\pi\nu)} \approx \varepsilon''(2\pi\nu) \quad (1)$$

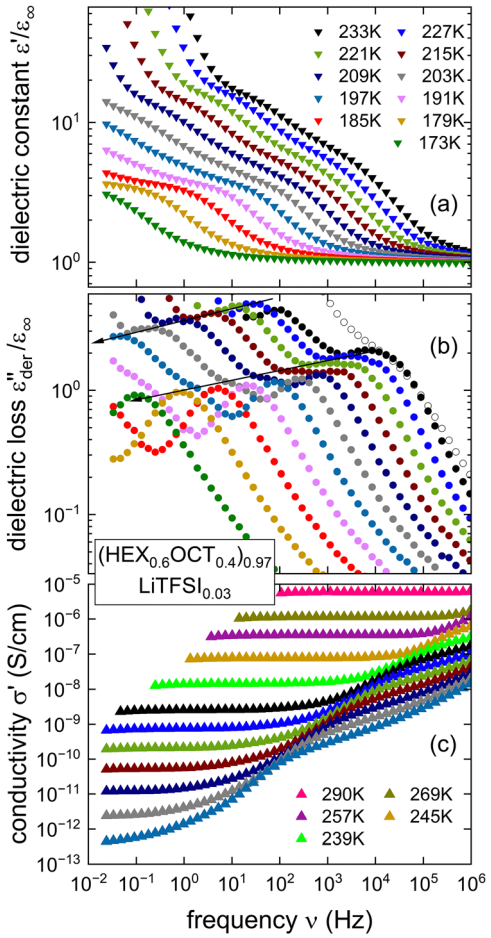

Fig. 1 Frequency dependent measurements of (a) the real part of the complex permittivity ε', (b) the imaginary part ε''_{der} of the normalized complex permittivity, and (c) the real part of the electrical conductivity σ' of $(HEX_{0.6}OCT_{0.4})_{0.97}(LiTFSI)_{0.03}$. In frame (b), the two left-pointing arrows are meant to highlight the temperature dependence of the two peaks that are resolved for most ε''_{der} spectra; for 233 K, the open symbols reflect ε'', *i.e.*, the dielectric loss prior to taking the derivative. The legend of frame (c) lists only the temperatures that are not given already in frame (a).

provides a suitable tool to suppress the impact of electrical conductivity on the appearance of the dielectric loss spectra. From Fig. 1(b), double-peak structures are indeed found for ε''_{der}. The high-frequency peaks are narrower than the low-frequency loss peaks. Their line shape is, however, hard to define because at the lowest frequencies, an upturn is found in ε''_{der}. This upturn, like the corresponding feature in ε', arises as a consequence of electrode polarization effects. Roughly two decades above the peak frequency, the high-frequency flanks of ε''_{der} exhibit a cross-over to a weaker frequency dependence. This may well indicate the presence of a secondary relaxation process, as reported for $HEX_{0.6}OCT_{0.4}$ doped with $LiPF_6$.[25] A close inspection of ε''_{der} reveals that the low-frequency peaks are slightly more temperature dependent than the high-frequency peaks. In other words, the two peaks are somewhat more separated at lower temperatures than they are at higher temperatures.

The representations in Fig. 1(a) and (b) clearly resolve dielectric relaxation steps and peaks. Fig. 1(c) shows the evolution of the real part, $\sigma'(\nu)$, of the complex, frequency-dependent electrical conductivity, $\sigma^*(\nu) = i\omega\varepsilon_0\varepsilon^*(\nu)$, where ε_0 designates the electrical field constant. The dc conductivity can easily be identified from the plateau $\sigma_{dc} = \sigma'(\nu \rightarrow 0)$. In the representation of Fig. 1(c), only the high-frequency relaxation process is evident, showing up as a shoulder, while the low-frequency process is superimposed by the dc contribution.

Before discussing corresponding relaxation times and conductivities for a doping level of 1 mol% and analyzing them in Section 4, in Fig. 2, we plot the dielectric loss as a function of temperature for several Li salt concentrations and several frequencies. When comparing the cooling with the heating runs for $(HEX_{0.6}OCT_{0.4})_{0.99}(LiTFSI)_{0.01}$ (see Fig. 2(a)), a well-developed hysteresis is seen to occur at temperatures between 265 and 278 K. Similar effects, yet with a less pronounced hysteresis, were obtained for c = 3 and 5 mol%, as shown in Fig. 2(b) and (c), respectively. For the 1% sample, a well-defined discontinuity shows up in ε'' which signals the presence of a phase transition, while for the 3% sample, the dielectric loss displays only a mild change of slope. For 5 mol%, hardly any such feature is discernible. Furthermore, for higher Li concentrations, clear signatures for liquid-to-crystal transitions are typically lacking.

For the 1% sample, the frequency and temperature dependent dielectric losses clearly reveal the presence of a relaxation process, showing up as a peak in $\varepsilon''(T)$, as seen in Fig. 2(a).

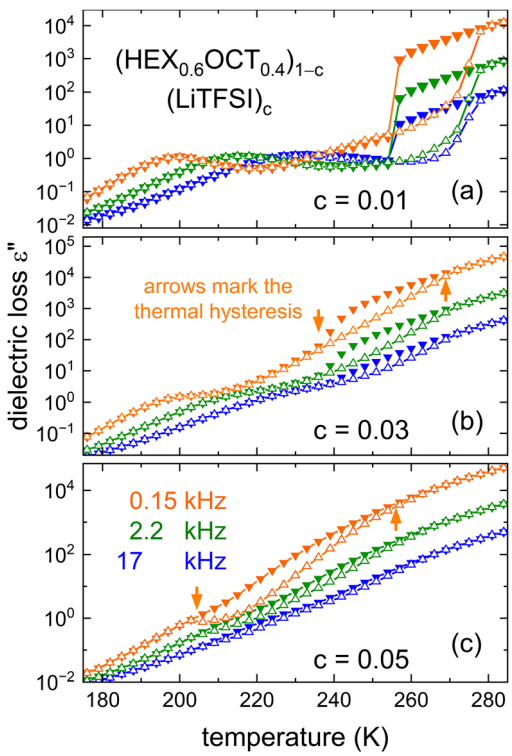

Fig. 2 Dielectric loss of $(HEX_{0.6}OCT_{0.4})_{1-c}LiTFSI_c$ as measured for several frequencies upon cooling (solid triangles pointing down) or heating (open triangles pointing up) for mole fractions c of (a) 1%, (b) 3%, and (c) 5%. The lines are guides to the eye. The arrows emphasize the hysteretic behavior that is most pronounced for the lowest frequency.

Indications for a relaxation process are also visible for $(HEX_{0.6}OCT_{0.4})_{0.97}(LiTFSI)_{0.03}$, as shown in Fig. 2(b). However, here the double peak structure in ε''_{der} that is clearly resolved from Fig. 1(b) is obviously obscured by the electrical conductivity.

Stronger Li doping: deep-eutectic regime

Dielectric results. For $(HEX_{0.6}OCT_{0.4})_{0.95}(LiTFSI)_{0.05}$, *i.e.*, for a larger salt concentration and thus higher expected electrical conductivity, a relaxation process is not at all apparent in the temperature range covered by Fig. 2(c). However, when plotting the frequency-dependent dielectric constant, as shown in Fig. 3(a), well-defined relaxation steps are obvious. This is because ε' (apart from blocking electrode effects) is insensitive to the electrical conductivity. Thus, by virtue of eqn (1) and after plotting the resulting (derivative) dielectric losses in the temperature range included in Fig. 2(c), Fig. 3(b) reveals well-defined, single-peaked dielectric loss curves.

Different from the loss curves seen for the plastic $(HEX_{0.6}OCT_{0.4})_{0.97}(LiTFSI)_{0.03}$ crystal in Fig. 2(b), those seen in Fig. 3(b) for $(HEX_{0.6}OCT_{0.4})_{0.95}(LiTFSI)_{0.05}$ display a clearly asymmetric shape that is rather expected for a supercooled liquid. From the high-frequency flanks of these asymmetric loss peaks, one recognizes that they become less steep and thus the spectra broader, as the sample is cooled. From Fig. 3(a), a Curie-type behavior is seen for the dielectric constant, *i.e.*, the relaxation steps increase somewhat with decreasing temperature.

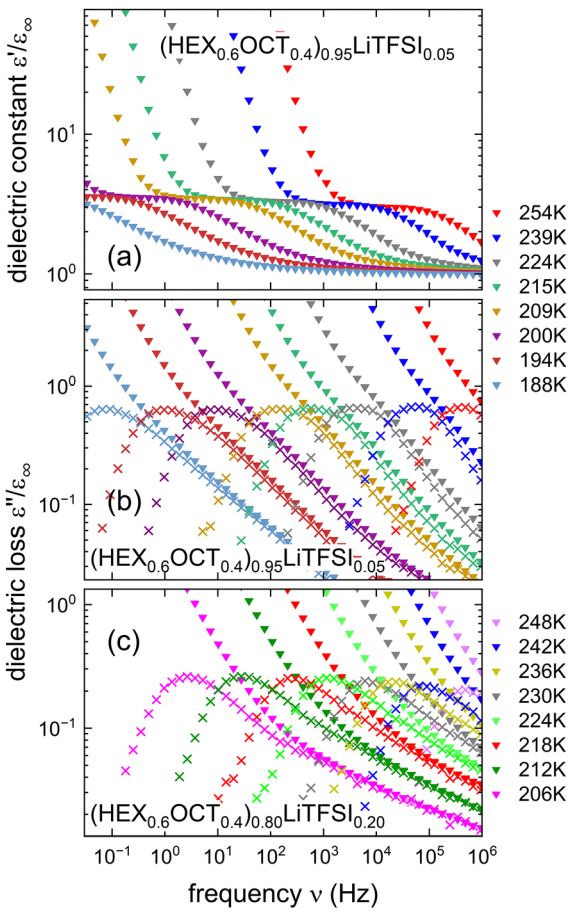

Fig. 3 (a) Real part, ε', and (b) imaginary part (ε'', triangles; ε''_{der}, crosses) of the normalized complex permittivity of $(HEX_{0.6}OCT_{0.4})_{1-c}(LiTFSI)_c$ for c = 5 mol%. (c) Normalized dielectric loss of a sample with c = 20 mol%. With the intention to highlight the differences between the dielectric spectra of the 3 mol% and 5 mol% samples, the ε' scale in frame (a) is chosen similar to that in Fig. 1(a).

The pattern observed for c = 5 mol% is similarly also found for higher Li salt concentrations. In particular for $c \geq 5$ mol%, there are no indications of double steps or peaks, nor do we observe compelling indications for structural phase transformations that would take place upon cooling. Fig. 3(c) shows the dielectric loss for $(HEX_{0.6}OCT_{0.4})_{0.80}(LiTFSI)_{0.20}$, *i.e.*, for a liquid with a much larger salt content. The ESI† provides a comparison with measurements for (binary) $HEX_{0.80}LiTFSI_{0.20}$ and $OCT_{0.80}LiTFSI_{0.20}$ mixtures. The relaxation times and the dc conductivities extracted from the various spectra will be discussed in Section 4.

NMR spectroscopy. While dielectric spectroscopy is sensitive to the integrated response of all dipolar and charge degrees of freedom, by virtue of isotope selectivity, NMR can provide access to the motions of specific ions or molecular segments. Here, we employ deuteron NMR to probe the reorientational dynamics of HEX-d_{11} (deuteron labeled at the carbon sites). Proton-detected diffusometry is used to track the long-range transport of the cycloalcohol molecules. Likewise, to be sensitive specifically to the lithium ion dynamics, we exploit ^{7}Li NMR. In the present situation, the advantage of the latter technique is limited by its relative insensitivity. This circumstance precluded us from exploring samples with Li-salt concentrations of less than 5 mol%. Furthermore, since dielectric spectroscopy yielded qualitatively relatively similar results for all samples with $c \geq 5$ mol% and in view of the long acquisition times that the ^{7}Li measurements require, we decided not to study samples with salt fractions beyond 5 mol%.

Using standard inversion or saturation procedures, we recorded the time evolution of the longitudinal magnetization recovery, $M_z(t)$. To determine the spin–lattice relaxation time T_1, we parameterized $M_z(t)$ using the stretched exponential function

$$M_z(t) = M_0 + (M_i - M_0)\exp[-(t/T_1)^{\mu}]. \quad (2)$$

In eqn (2), M_i and M_0 denote the initial and the equilibrium magnetization, respectively, and the Kohlrausch exponent μ describes the stretching of the spin–lattice relaxation. Fig. 4(a) and (b) summarize the exponents μ and the T_1 times, respectively, of $(HEX_{0.6}OCT_{0.4})_{0.95}(LiTFSI)_{0.05}$. For 210 K $< T <$ 225 K, the dephasing of the transverse magnetization, *i.e.*, the spin–spin relaxation (see the ESI†) was so fast that reliable T_1 measurements could not be performed. Fig. 4(b) shows that well-defined T_1 minima occur for the ^{2}H as well as the ^{7}Li probe.

At the temperatures of the T_1 minima, motional correlation times τ_c can be estimated from the relation $\omega_L\tau_c = 0.62$.[47] This relation rationalizes, at least partially, why for ^{7}Li (for which the Larmor frequency ω_L is about 2.5 times greater than for ^{2}H), the T_1 minimum appears at a temperature that is larger than it is for the deuterons. A discussion of the resulting correlation

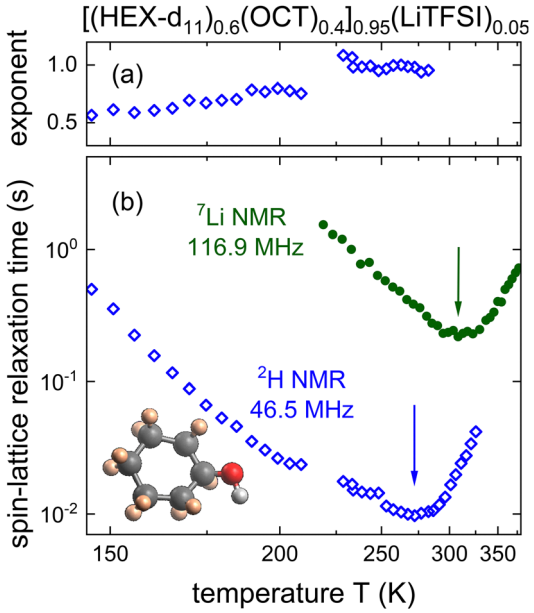

Fig. 4 Temperature dependent (a) Kohlrausch exponents and (b) ^{2}H (diamonds) and ^{7}Li (circles) spin–lattice relaxation times of $(HEX\text{-}d_{11})_{0.6}(OCT)_{0.4}$ doped with 5 mol% LiTFSI. The arrows mark the approximate positions of the T_1 minima near 272 K (for ^{2}H) or 308 K (for ^{7}Li). Kohlrausch exponents are shown only for temperatures for which the magnetization curves deviate significantly from an exponential behavior. A sketch of the HEX-d_{11} molecule is given, where the deuteron labeled sites are marked by light coloring.

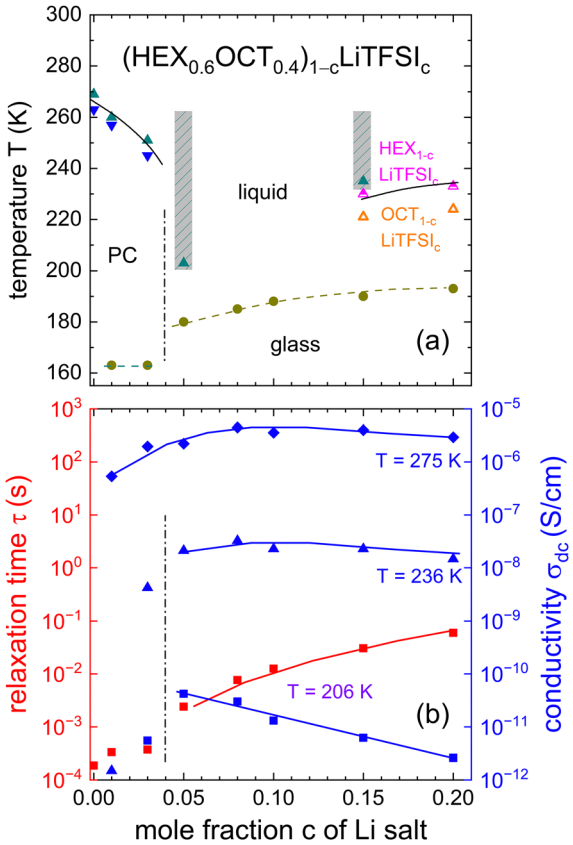

Fig. 5 (a) Compilation of transition temperatures obtained during cooling (triangles pointing downward) or heating (triangles pointing upward). The hatching indicates that only during warm-up, hints of a transition appeared. The circles mark temperatures with dielectric reorientation times of 100 s which signal a freezing of the molecular orientations on this scale, *i.e.*, they indicate glass transitions. (b) Concentration-dependent conductivities are given for several temperatures. Dipolar reorientation times are shown for 206 K. In both frames, the lines are guides to the eye. Across the dash-dotted line, which separates the plastic-crystal from the glass-former regime, one notes jumps in T_g, σ_{dc}, and τ.

times, also in relation to the ones from dielectric spectroscopy, will be given in Section 4.

Fig. 4(a) presents the Kohlrausch exponents that characterize the magnetization curves, however, only if the exponents differ markedly from $\mu = 1$. As one infers from Fig. 4(a), this is the case only for the ^{2}H spin–lattice relaxation at $T < 220$ K. In that range, μ decreases upon cooling, indicating an increasingly wider distribution of T_1 times. Since here we are in the slow-motion regime, $\omega_L\tau_c \gg 1$, this increase indicates that the τ_c distribution broadens. This observation is compatible with the broadening of the ε'' spectra of $(HEX_{0.6}OCT_{0.4})_{0.95}(LiTFSI)_{0.05}$ that was noted in the context of Fig. 3(b).

4. Discussion

With the goal to map out the phase behavior of the $(HEX_{0.6}OCT_{0.4})_{1-c}(LiTFSI)_c$ system, Fig. 5(a) compiles the temperatures that were inferred from the hysteretic behavior in ε'' such as shown in Fig. 2. For salt concentrations $c < 5$ mol%, the crystallization and melting temperatures of the mixtures strongly decrease as c increases. Furthermore, for the two Li-doped PCs (with $c = 1$ mol% and 3 mol%) that we measured in this low-c regime, the orientational freezing on the 100 s scale is *in*dependent of c. By contrast, for larger salt concentrations, the $(HEX_{0.6}OCT_{0.4})_{1-c}(LiTFSI)_c$ samples do *not* crystallize upon cooling. Hence, the 100 s-freezing, now corresponding to a liquid-to-glass transition, takes place at successively higher temperatures as c increases. This $T(c)$ behavior resembles the one reported for other structural glass formers that contain a substantial amount of LiTFSI.[21,29]

The weak hysteretic behavior observed for some mixtures with $c \geq 5$ mol%, in Fig. 5(a) highlighted by hatching, calls for particular consideration. Fig. 2(c) shows that the dielectric loss of $(HEX_{0.6}OCT_{0.4})_{0.95}(LiTFSI)_{0.05}$ evolves smoothly upon cooling, Yet, as expected from so-called two-step crystallization experiments,[48] the nucleation propensity is generally increased by deep prior undercooling. Hence, in reheating runs, crystallization becomes more likely, in harmony with the observations made from Fig. 2(c) for the 5 mol% sample. The hatching marks the hysteretic range also for $(HEX_{0.6}OCT_{0.4})_{0.85}(LiTFSI)_{0.15}$. The ESI† shows that $HEX_{1-c}LiTFSI_c$ and $OCT_{1-c}LiTFSI_c$ with $c = 15$ and 20 mol% display similar effects.

Interestingly, the phase diagram shown in Fig. 5(a) resembles those of some LiTFSI-dinitrile systems.[21] For the doped cycloalcohols, this observation suggests that near $c \approx 10$ mol%, the presumed eutectic point is so low that crystallization is effectively inhibited also upon reheating.

It is not only instructive to plot isochronal quantities such as in Fig. 5(a), but it is also revealing to consider the concentration dependence of the time scales τ as well as of the electrical conductivities σ_{dc} in an isothermal fashion. This is shown in Fig. 5(b). Here, one recognizes that at 275 K, *i.e.*, above the temperatures at which even the neat cycloalcohols become solid, the ionic conductivity σ_{dc} displays a maximum near $c = 10$ mol%. This σ_{dc} maximum, appearing at a molarity of about 1 M, is a remarkable finding. It is not completely unexpected, though, since numerous other liquid electrolytes also exhibit a σ_{dc} maximum near 1 M salt concentrations.[21,29,32,49,50] Our σ_{dc} data at 236 K are not incompatible with such a feature, but also not fully compelling in that respect.

Recalling that the PC state is stable for $c < 5$ mol%, it is seen that σ_{dc} is significantly lower in the crystalline solid than the value extrapolated from the liquid (*i.e.*, from the data for $c \geq 5$ mol%). For 206 K, σ_{dc} of $(HEX_{0.6}OCT_{0.4})_{0.97}(LiTFSI)_{0.03}$ is again relatively small; for the 1 mol% sample, it is about 2×10^{-14} S cm^{-1}, *i.e.*, too low to be within the range shown in Fig. 5(b).

The isothermal relaxation times (at $T = 206$ K), shown in Fig. 5(b), and the isochronal relaxation times (at $\tau = 10^2$ s), shown in Fig. 5(a), indicate the same trend as a function of the molar salt fraction c: for $c < 5$ mol%, τ, and correspondingly T_g, do not significantly change with c, while for larger salt concentrations, an increase of τ and of T_g is seen to emerge.

To obtain an overview regarding the translational and reorientational dynamics in a large temperature range, Fig. 6 presents the relaxation times and the inverse conductivity, *i.e.*, the dc resistivity $\rho_{dc} = 1/\sigma_{dc}$, in an Arrhenius fashion. Frame (a) focuses on samples with $c < 5$ mol%. Including data also for undoped $HEX_{0.6}OCT_{0.4}$ and for $LiPF_6$ doping,[25] it is seen that the presence of Li salt leads to only mild changes in the reorientational dynamics. In ref. 25, the latter was identified as the so-called α-dynamics. It is important to realize that we determined τ_α from the high-frequency peaks of the double-peak structures that are seen for $(HEX_{0.6}OCT_{0.4})_{0.97}(LiTFSI)_{0.03}$ in Fig. 1(b).

To elucidate the nature of the low-frequency peaks, the corresponding time scales, that will be called τ_{ion}, are also included in Fig. 6(a). One recognizes that they display a somewhat stronger temperature dependence than τ_α, which, however, matches that of the dc resistivity very well. To emphasize this coincidence, the resistivity and the relaxation ordinate axes were shifted accordingly. The striking similarity to the behavior seen for LiTFSI-doped adamantane-based PCs[27] strongly suggests that the slower-than-α process is also here due to the ion transport. This is why, like in ref. 27, the corresponding relaxation time are designated τ_{ion}. Ref. 27 points out that in most ion conductors the observation of this feature is hampered by the presence of spectrally close reorientational contributions. In the ESI,† the dielectric spectra of $(HEX_{0.6}OCT_{0.4})_{0.99}(LiTFSI)_{0.01}$ are also seen to display a double-peak structure and for this sample, Fig. 6(a) reveals a close thermal evolution of τ_{ion} and ρ_{dc} as well. Hence, one may ask whether the observation of an ion-transport dielectric loss peak in PCs is particularly facilitated by the presence of the LiTFSI salt.

To address this question, we analyzed unpublished raw data[25] for $(HEX_{0.6}OCT_{0.4})_{0.99}(LiPF_6)_{0.01}$, a cycloalcohol mixture

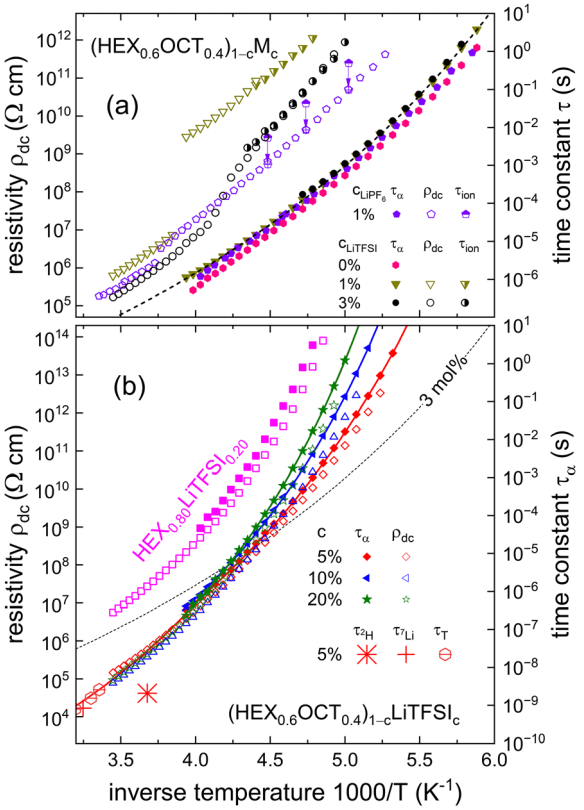

Fig. 6 Arrhenius plot of resistivity ρ_{dc} (open symbols) and relaxation times (τ_α as filled symbols and τ_{ion} as half-filled symbols, both derived from inverse circular peak frequencies) for $HEX_{0.6}OCT_{0.4}$ doped (a) at mole fractions (a) of $c < 5$ mol% and (b) at larger levels. Frame (a) features data relating to LiTFSI doping as well as results of a sample devoid of added salt. The purple pentagons represent data (based on ref. 25) for a crystal doped with 1 mol% of $LiPF_6$. In frame (a), the ordinate axes are shifted so that for $(HEX_{0.6}OCT_{0.4})_{0.97}(LiTFSI)_{0.03}$ the τ_{ion} and the ρ_{dc} data overlap. Frame (b) shows ρ_{dc} and τ_α for $(HEX_{0.6}OCT_{0.4})_{1-c}(LiTFSI)_c$ with $c = 5$, 10, and 20 mol% as well as for $HEX_{0.80}LiTFSI_{0.20}$. For visual clarity, the latter data are shifted upward by 2 decades. Also included are NMR-based motional times inferred from the ^{2}H (asterisk) and ^{7}Li (plus sign) T_1 minima reported in Fig. 4, as well as the diffusion-based translational times τ_T (hexagons with horizontal bars). All lines in the present figure are guides to the eye. In both frames, the *y*-axes are adjusted so that all decade ticks are spaced equally. Thus, by construction, the relative shift of the ρ_{dc} and the τ axes in frame (a) differs from that chosen for frame (b).

featuring another Li salt. For that sample, careful scrutiny also reveals a double-peak structure in ε''_{der}, implying that this feature may be more general than previously thought. The temperature dependence of the corresponding slower-than-α time scale, τ_{ion}, is included in Fig. 6(a). It matches the temperature dependence of the electrical resistivity excellently. However, the relative shift of the ordinate axes (chosen to lead to an overlap of τ_{ion} and ρ_{dc} for the LiTFSI based PCs) does not apply for the $LiPF_6$-based electrolytes. Here, overlap with ρ_{dc} is achieved by shifting the τ_{ion} symbols downward by an additional factor of 5 (see the arrows in Fig. 6(a)).

The necessity to use different sample-dependent shift factors, in order to generate an overlap of the ρ_{dc} and the τ data in Fig. 6(a), reminds one of the fact that ρ_{dc} and τ are

rather disparate quantities. Hence, a comparison between them is necessarily indirect. Relations among the conductivity relaxation time τ_D and $\rho_{dc} = 1/\sigma_{dc}$ have variously been formulated, *e.g.*, as $\sigma_{dc}\tau_D = \varepsilon_0\varepsilon_\infty$ or in terms of the empirical Barton-Nakajima-Namikawa rule, $\sigma_{dc}\tau_D = p\varepsilon_0(\varepsilon_s - \varepsilon_\infty)$, where p is a constant close to 1 and ε_s is the static dielectric constant.[51,52] There is some debate regarding the assignment of ε_s in ionic systems.[53] It is clear, however, that the proportionality constants between τ_D and ρ_{dc} can vary quite a bit and that they can be (weakly) temperature dependent as well. Furthermore, it has been asserted that "the conductivity relaxation time τ_D is proportional to, not equal to, the ionic hopping correlation time".[54] Thus, in order to enable a direct, quantitative comparison of translational with reorientational or structural time scales, all these circumstances suggest to employ τ_{ion} based, rather than σ_{dc} based measures, whenever possible.

For $(HEX_{0.6}OCT_{0.4})_{0.97}(LiTFSI)_{0.03}$, Fig. 6(a) indicates that τ_α and τ_{ion} share similar temperature dependences. A closer look reveals, however, an increasing dynamic decoupling between these quantities as the sample is cooled. In Fig. 6(a), the decoupling for this crystal is seen to be considerably more pronounced than it is for 1 mol%. This becomes particularly clear, if one observes that for c = 1 and 3 mol% of LiTFSI doping, the temperature dependences of τ_α are practically identical. At the same time, for c = 3 mol%, the temperature dependence of τ_{ion} is significantly steeper than that for the 1 mol% sample.

However, the dynamic decoupling, even for the 3 mol% crystal, is still much less pronounced than that reported for LiTFSI-doped adamantane.[27] There, τ_α shows only minor deviations from an Arrhenius temperature dependence, while τ_{ion} displays a pronounced super-Arrhenius behavior. The latter has been taken to indicate an appearance of glassy dynamics in the ionic subsystem which has been rationalized within various approaches.[55–58] Significant deviations from thermally activated behavior are not obvious in the relatively small range in which τ_{ion} could be detected for the 3 mol% sample. Yet, for $(HEX_{0.6}OCT_{0.4})_{0.97}(LiTFSI)_{0.03}$, an Arrhenius-based extrapolation of τ_{ion} toward high temperatures yields an attempt frequency in excess of 10^{20} Hz. Such "unrealistically" large values are usually considered as a smoking gun for non-Arrhenian behavior. The presently discussed 1 mol% samples, *i.e.*, $(HEX_{0.6}OCT_{0.4})_{0.99}(LiPF_6)_{0.01}$ and $(HEX_{0.6}OCT_{0.4})_{0.99}(LiTFSI)_{0.01}$, display less pronounced decoupling effects, as shown in Fig. 6(a).

In the $c \geq 5$ mol% regime, *i.e.*, for higher doping levels, Fig. 6(b) reveals a different kind of behavior. Here, the reorientational dynamics within the matrix, *i.e.*, the α relaxation time, does significantly depend on the salt content as the glass transition is approached. Conversely, for higher temperatures, τ_α depends little on c. As representative examples, Fig. 6(b) comprises τ_α data for samples with c = 5, 10, and 20 mol% (also data for $HEX_{0.80}$-$LiTFSI_{0.20}$ are included; for additional compositions, see the ESI†). To examine the relation of τ_α and the ion hopping times, the time constant τ_{Li} extracted from the ^{7}Li T_1 minimum is added to Fig. 6(b). One recognizes that τ_{Li} smoothly lines up with τ_α, strongly suggesting a coupling of reorientational and translational time scales. Using this finding, in Fig. 6(b), the ρ_{dc} axis was adjusted (relative to the τ_α axis) accordingly. The common representation of τ_α and ρ_{dc} that is embodied in this figure shows that toward lower temperatures, a rather weak decoupling of the rotational from the translational degrees emerges, which remains much smaller than in the plastic-crystal regime.

A more succinct and more common way to check for a possible (de-) coupling of conductivity and reorientational dynamics is to plot the dc resistivity ρ_{dc} *versus* the dipolar relaxation time τ in a double-logarithmic representation.[59–62] If the two dynamics are coupled, in the sense that they display the same temperature dependence, a power law $\rho_{dc} \propto \tau^\xi$ with an exponent ξ = 1 is expected. Indeed, for a host of choliniumchloride and Li-salt based deep eutectic solvents, the experimentally determined exponents are in the range $0.9 < \xi < 1.1$.[63] Fig. 7 shows that such a power-law behavior, with ξ = 0.92, is found for the c = 5 mol% electrolyte, *i.e.*, in the deep-eutectic-solvent regime. Conversely, for c = 3 mol%, we find ξ = 1.8. This result confirms the observation made from Fig. 6(a) that severe deviations from rotation-translation coupling emerge when transitioning from the glass-forming to the PC regime.

Returning to the deep-eutectic-solvent regime, in the present work, we employ proton-detected diffusometry to trace the translational motions of the cycloalcohol molecules within the 5 mol% sample. To directly compare the self-diffusion coefficients D_{trans} (tabulated in the ESI†) with the time constants in Fig. 6(b), we exploit the Stokes–Einstein-Debye relation. This involves the solution of the rotation diffusion equation in terms of the Legendre polynomials P_ℓ. In the NMR context, the correlation times refer to polynomials of rank ℓ = 2. The resulting Stokes–Einstein-Debye relationship implies a coupling of the rotational diffusion coefficient[64,65]

$$D_{rot} = \frac{k_B T}{8\pi\eta R_H^3} = \frac{1}{\ell(\ell+1)\tau} = \frac{1}{6\tau} \quad (3)$$

and the translational diffusion coefficient

$$D_{trans} = \frac{k_B T}{6\pi\eta R_H} = \frac{4}{3} R_H^2 D_{rot}, \quad (4)$$

here given in the limit of stick boundary conditions. In these expressions, η denotes the shear viscosity and R_H denotes the hydrodynamic radius. By thus assuming a coupling of the rotational and translation dynamics, one arrives at a "translational diffusion time"[66,67]

$$\tau_T = \frac{2R_H^2}{9D_{trans}}. \quad (5)$$

To achieve coincidence of τ_T with the other translational time scales appearing in Fig. 6(b), we assumed a hydrodynamic radius of R_H = 2.1 Å. Often R_H is close to the molecular van der Waals radius R_{vdW}.[64] From ref. 68, the latter quantity can be estimated to be 2.97 Å for HEX and 3.25 Å for OCT so that R_{vdW} for $HEX_{0.6}OCT_{0.4}$ amounts to about 3.1 Å. The finding that $R_{trans} < R_{vdW}$ for most liquids, in particular for those formed by internally flexible molecules, is well known.[64,65] It has also been pointed out[65] that the use of slip boundary conditions is "resulting in R_H values larger by a factor of 1.5."

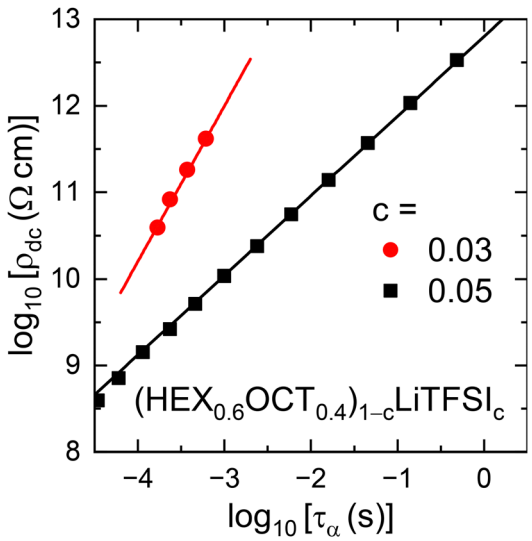

Fig. 7 This plot shows for $(HEX_{0.6}OCT_{0.4})_{0.95}(LiTFSI)_{0.05}$ that the dc resistivity ρ_{dc} is essentially proportional to the relaxation time τ_α as revealed by the black line with a slope of 0.92. For $(HEX_{0.6}OCT_{0.4})_{0.97}(LiTFSI)_{0.03}$, however, the much increased power-law slope (red line) indicates a significant decoupling of the rotational from the translational degrees of freedom.

Initially, we expected that the deuteron NMR measurements of the HEX-d_{11} molecules, that we carried out for the 5 mol% sample, are most sensitive to their overall reorientational dynamics. Viewed from that perspective, it is somewhat surprising that the deuteron T_1 minimum implies a time scale that is much shorter than expected from the dielectric τ_α times, as shown in Fig. 6(b). This observation thus hints at the importance of other (faster) motional processes with conformational modulations of the molecules as a potential candidate.[69–71] The most likely scenario is indicated by proton and carbon T_1 measurements of neat HEX crystals.[39] These experiments revealed a type of motion that was described as a "uniaxial internal rotation of the cyclohexyl ring about the CO bond, with the COH group remaining stationary,"[39] so that this process was concluded to display an, at best, weak dielectric signature. Hence, the dielectric response is governed by the collective reorientational molecular motions (*i.e.*, the α-process).[25] Thus, similar to previous work,[7,11,23] the charge motions are envisioned to be facilitated by the global reorientational motions of the whole molecules.

As we have seen, for the glass forming liquids studied in this work, a double-peak in their dielectric dispersion, *i.e.*, a resolved translational loss peak is not detected. This contrasts with the findings for the previously[27] and the presently studied salt-doped PCs. The observation of a translational loss peak is, however, not generally restricted to PCs. It is for instance also observable for ionic glass formers devoid of constituents which by symmetry lack electrical dipole moments. Some molten salts like $2Ca(NO_3)_2$-$3KNO_3$[72] and other glassy electrolytes[73–76] fall within this category. Interestingly, also for an ionic liquid composed solely of symmetric ions, the dielectric loss peaks were "ascribed to the frequency-dependent translational motion of ions, rather than the coupling with the reorientational relaxation."[77]

5. Conclusions

In the present work, we studied the relationship of reorientational dynamics and charge transport in LiTFSI-doped cycloalcohols. Dielectric and conductivity measurements were carried out for salt concentrations ranging from 1 to 20 mol%. Close to room temperature, a conductivity maximum exists near the 1 M molarity, corresponding to about 10 mol% of salt doping. Upon cooling, a more complex behavior emerges. It is found that for $c < 5$ mol% at low temperatures, orientationally disordered crystals are stable. For them, we observe a two-step dielectric function. In harmony with previous work, also on undoped cycloalcohols, the high-frequency process is identified as the one which drives orientational freezing. By contrast, the low-frequency process corresponds to the ion transport. Its observation is not unprecedented (see ref. 27), but somewhat uncommon, and the present work reveals that it may be more abundant than previously thought. A prerequisite for its unambiguous detection is that reorientational processes must not overshadow nearby ionic relaxations. Promising for their observation is thus the study of strongly decoupled ion conductors and ion conductors for which the reorientation related contributions are small or even absent. This is not only the case for the presently studied crystals, but, as discussed, also for some molten salts and various glassy electrolytes.

For the reorientational and the translational degrees of freedom of lightly Li-doped $HEX_{0.6}OCT_{0.4}$, we detected weak but significant differences of their temperature dependences. This is similar to the findings for some other Li-doped cycloalcohol mixtures that are based on comparing conductivities and motional time scales.[25] Reorientational and translational time scales that evolve differently with temperature point to a decoupling of the underlying degrees of freedom. The observation of different thermal evolutions precludes a perfect one-to-one coupling as expected if a "revolving-door" mechanism would dominate the ionic conductivity of these systems. However, as we pointed out, any comparison between time scales and conductivities is necessarily indirect. Conversely, following ref. 27, here, based on the directly determined time constant τ_{ion}, we were able to perform a more direct comparison of the ionic and structural time scales. The degree of decoupling that we thus find in the Li-doped cycloalcohols is certainly much less pronounced than in Li-doped adamantane-based PCs,[27] a finding which in ref. 27 was rationalized by the more globular shape of the molecules in those systems.

The situation is different for salt concentrations of 5 mol% and more. Here, all the samples display a liquid-to-glass transition rather than an orientational glass transition. The overall phase behavior reveals a concentration-temperature pattern that resembles the one known from deep eutectic solvents.

For $(HEX_{0.6}OCT_{0.4})_{0.95}(LiTFSI)_{0.05}$, we combined dielectric spectroscopy to probe the reorientational motions with ^{7}Li NMR as well as diffusometry to probe the cationic and molecular (cycloalcohol) transport, respectively. At least near room temperature, where the NMR results were exploited to obtain absolute translational time scales, τ_T, we demonstrated a close

coupling of the reorientational and translational dynamics. In addition, the comparison with the conductivity of the glass forming samples also indicates that towards lower temperature, the coupling of reorientations and translations remains relatively close. As discussed, *e.g.*, in ref. 61 for particles moving within a viscous liquid, such a behavior is predicted by the combined Stokes–Einstein, Stokes–Einstein-Debye, and Nernst–Einstein relations. Within this framework, the observed rotation-translation coupling arises from the direct relation of both the rotational and the translational diffusion times, *cf.* eqn (3) and (4), to the viscosity. In contrast, for the plastic-crystalline states found at low salt concentrations in the present work, such viscosity-mediated coupling is excluded and a different type of rotation-translation coupling, most likely *via* the "revolving-door" mechanism, has to be invoked. Our results show that in the investigated cycloalcohol PCs with low salt content, this mechanism leads to less perfect coupling than for the samples with high salt content, where the viscosity-mediated mechanism is active. To summarize, our study reveals how small compositional changes can be exploited to tune a transition of Li-doped cycloalcohols from PCs with less coupled dynamics to glass forming liquids with largely coupled motions.

Conflicts of interest

There are no conflicts of interest to declare.

Data availability

The data presented in this article are all given in the manuscript figures. Data supporting this article are part of the ESI† and are shown there as figures and tables.

Acknowledgements

This work was financially supported by the Deutsche Forschungsgemeinschaft under Project No. 429918288 and 444797029.

References

1 N. S. Grundish, J. B. Goodenough and H. Khani, Designing composite polymer electrolytes for all-solid-state lithium batteries, *Curr. Opin. Electrochem.*, 2021, **30**, 100828.
2 S. Kundu and Y. Ein-Eli, A review on design considerations in polymer and polymer composite solid-state electrolytes for solid Li batteries, *J. Power Sources*, 2023, **553**, 232267.
3 G. P. Pandey, T. Liu, C. Hancock, Y. Li, X. S. Sun and J. Li, Thermostable gel polymer electrolyte based on succinonitrile and ionic liquid for high-performance solid-state supercapacitors, *J. Power Sources*, 2016, **328**, 510–519.
4 Q. Li, F. Yan and J. Texter, Polymerized and Colloidal Ionic Liquids–Syntheses and Applications, *Chem. Rev.*, 2024, **124**, 3813–3931.
5 J. Hwang, K. Matsumoto, C.-Y. Chen and R. Hagiwara, Pseudo-solid-state electrolytes utilizing the ionic liquid family for rechargeable batteries, *Energy Environ. Sci.*, 2021, **14**, 5834–5863.
6 Y. Kato, S. Hori, T. Saito, K. Suzuki, M. Hirayama, A. Mitsui, M. Yonemura, H. Iba and R. Kanno, High-power all-solid-state batteries using sulfide superionic conductors, *Nat. Energy*, 2016, **1**, 16030.
7 E. I. Cooper and C. A. Angell, Ambient temperature plastic crystal fast ion conductors (PLICFICS), *Solid State Ionics*, 1986, **18–19**, 570–576.
8 T. Bauer, M. Köhler, P. Lunkenheimer, A. Loidl and C. A. Angell, Relaxation Dynamics and Ionic Conductivity in a Fragile Plastic Crystal, *J. Chem. Phys.*, 2010, **133**, 144509.
9 Z. Zhang and L. F. Nazar, Exploiting the paddle-wheel mechanism for the design of fast ion conductors, *Nat. Rev. Mater.*, 2022, **7**, 389–405.
10 P.-J. Alarco, Y. Abu-Lebdeh, A. Abouimrane and M. Armand, The plastic-crystalline phase of succinonitrile as a universal matrix for solid-state ionic conductors, *Nat. Mater.*, 2004, **3**, 476–481.
11 D. R. MacFarlane and M. Forsyth, Plastic crystal electrolyte materials: New perspectives on solid state ionics, *Adv. Mater.*, 2001, **13**, 957–966.
12 A. Abouimrane and I. J. Davidson, Solid Electrolyte Based on Succinonitrile and LiBOB: Interface Stability and Application in Lithium Batteries, *J. Electrochem. Soc.*, 2007, **154**, A1031–A1034.
13 H. Zhu, D. R. MacFarlane, J. M. Pringle and M. Forsyth, Organic Ionic Plastic Crystals as Solid-State Electrolytes, *Trends Chem.*, 2019, **1**, 126–140.
14 I. S. Klein, Z. Zhao, S. K. Davidowski, J. L. Yarger and C. A. Angell, A New Version of the Lithium Ion Conducting Plastic Crystal Solid Electrolyte, *Adv. Energy Mater.*, 2018, **8**, 1801324.
15 S. Tian, B. Shao, Z. Wang, S. Li, X. Liu, Y. Zhao and L. Li, Organic ionic plastic crystal as electrolyte for lithium-oxygen batteries, *Chin. Chem. Lett.*, 2019, **30**, 1289–1292.
16 H. Zhou, S. Sato, Y. Nishiyama, G. Hatakeyama, X. Wang, Y. Murakami and T. Yamada, Molecular Design of Organic Ionic Plastic Crystals Consisting of Tetracyanoborate with Ultralow Phase Transition Temperature, *J. Phys. Chem. Lett.*, 2023, **14**, 9365–9371.
17 W. S. Tang, M. Matsuo, H. Wu, V. Stavila, W. Zhou, A. A. Talin, A. V. Soloninin, R. V. Skoryunov, O. A. Babanova, A. V. Skripov, A. Unemoto, S. I. Orimo and T. J. Udovic, Liquid-Like Ionic Conduction in Solid Lithium and Sodium Monocarba-closo-Decaborates Near or at Room Temperature, *Adv. Energy Mater.*, 2016, **6**, 1502237.
18 L. Jin, P. C. Howlett, J. M. Pringle, J. Janikowski, M. Armand, D. R. MacFarlane and M. Forsyth, An organic ionic plastic crystal electrolyte for rate capability and stability of ambient temperature lithium batteries, *Energy Environ. Sci.*, 2014, **7**, 3352–3361.
19 Y. Hirotsu, R. Sekiguchi, Y. Takeoka, M. Rikukawa and M. Yoshizawa-Fujita, Phase transition and ionic conductivity of pyrrolidinium-based ionic plastic crystals with magnesium salts, *Bull. Chem. Soc. Jpn.*, 2024, **97**, uoae101.

20 P. S. Whitfield, A. Abouimrane and I. J. Davidson, *In situ* XRD study of the succinonitrile–lithium bis(trifluoromethylsulfonyl) imide (LiTFSI) phase diagram, *Solid State Ionics*, 2010, **181**, 740–744.
21 Y. Ugata, R. Tatara, K. Ueno, K. Dokko and M. Watanabe, Highly concentrated $LiN(SO_2CF_3)_2$/dinitrile electrolytes: Liquid structures, transport properties, and electrochemistry, *J. Chem. Phys.*, 2020, **152**, 104502.
22 M. Zachariah, M. Romanini, P. Tripathi, J. L. Tamarit and R. Macovez, Molecular diffusion and dc conductivity perfectly correlated with molecular rotational dynamics in a plastic crystalline electrolyte, *Phys. Chem. Chem. Phys.*, 2015, **17**, 16053–16057.
23 K. Geirhos, P. Lunkenheimer, M. Michl, D. Reuter and A. Loidl, Communication: Conductivity enhancement in plastic-crystalline solid-state electrolytes, *J. Chem. Phys.*, 2015, **143**, 081101.
24 D. Reuter, P. Lunkenheimer and A. Loidl, Plastic-crystalline solid-state electrolytes: Ionic conductivity and orientational dynamics in nitrile mixtures, *J. Chem. Phys.*, 2019, **150**, 244507.
25 D. Reuter, C. Geiß, P. Lunkenheimer and A. Loidl, Variation of ionic conductivity in a plastic-crystalline mixture, *J. Chem. Phys.*, 2017, **147**, 104502.
26 S. Abeysooriya, F. Makhlooghiazad, J.-N. Chotard, L. A. O'Dell and J. M. Pringle, Investigation of the Physicochemical Properties of Pyrrolidinium-Based Mixed Plastic Crystal Electrolytes, *J. Phys. Chem. C*, 2023, **127**, 12304–12320.
27 D. Reuter, K. Seitz, P. Lunkenheimer and A. Loidl, Ionic conductivity and relaxation dynamics in plastic crystals with nearly globular molecules, *J. Chem. Phys.*, 2020, **153**, 014502.
28 A. Dorai, S. Kim, N. Kuwata, J. Kawamura, K. Kisu and S.-I. Orimo, Understanding Ion Dynamics in Closoborate-Type Lithium-Ion Conductors on Different Time-Scales, *J. Phys. Chem. Lett.*, 2024, **15**, 4864–4871.
29 S. Lansab, B. Grabe and R. Böhmer, Paddle-wheel mechanism in doped succinonitrile-glutaronitrile plastic electrolytes: A joint magnetic resonance, dielectric, and viscosimetry study of Li ion translational and molecular reorientational dynamics, *Phys. Chem. Chem. Phys.*, 2023, **25**, 9382–9393.
30 S. Davidowski, A. R. Young-Gonzales, R. Richert, J. Yarger and C. A. Angell, Relation of Ionic Conductivity to Solvent Rotation Times in Dinitrile Plastic Crystal Solvents, *J. Electrochem. Soc.*, 2020, **167**, 070553.
31 S. Lansab, T. Schwan, K. Moch and R. Böhmer, Shear rheology senses the electrical conductivity optimum in highly Li doped dinitrile electrolytes, *J. Chem. Phys.*, 2024, **160**, 084503.
32 C. J. Franko, C.-H. Yim, F. Aren, G. Avall, P. S. Whitfield, P. Johansson, Y. A. Abu-Lebdeh and G. R. Goward, Concentration Dependent Solution Structure and Transport Mechanism in High Voltage LiTFSI-Adiponitrile Electrolytes, *J. Electrochem. Soc.*, 2020, **167**, 160532.
33 B. B. Hansen, S. Spittle, B. Chen, D. Poe, Y. Zhang, J. M. Klein, A. Horton, L. Adhikari, T. Zelovich, B. W. Doherty, B. Gurkan, E. J. Maginn, A. Ragauskas, M. Dadmun, T. A. Zawodzinski, G. A. Baker, M. E. Tuckerman, R. F. Savinell and J. R. Sangoro, Deep Eutectic Solvents: A Review of Fundamentals and Applications, *Chem. Rev.*, 2021, **121**, 1232–1285.
34 Gangasharan and S. S. N. Murthy, Study of α-, β-, and γ-relaxation processes in some supercooled liquids and supercooled plastic crystals, *J. Chem. Phys.*, 1993, **99**, 9865–9873.
35 D. L. Leslie-Pelecky and N. O. Birge, Dielectric measurement of the model glass transition in orientationally disordered cyclo-octanol, *Phys. Rev. B: Condens. Matter*, 1994, **50**, 13250–13258.
36 R. Brand, P. Lunkenheimer and A. Loidl, Relaxations and fast dynamics of the plastic crystal cyclo-octanol investigated by broadband dielectric spectroscopy, *Phys. Rev. B: Condens. Matter*, 1997, **10**, R5713–R5716.
37 T. Eguchi, G. Soda and H. Chihara, Molecular motion and polymorphic forms in cyclohexanol as studied by nuclear magnetic resonance, *J. Magn. Reson.*, 1976, **23**, 55–65.
38 A. Dworkin, A. H. Fuchs, M. Ghelfenstein and H. Szwarc, Cristaux vitreux. I: RMN large bande, thermocourants de dépolarisation et analyse enthalpique dans quelques cycloalcools, *J. Phys. Lett.*, 1982, **43**, 21–27.
39 P. L. Kuhns and M. S. Conradi, NMR study of molecular motions in cyclohexanol, a glass-forming rotor crystal, *J. Chem. Phys.*, 1984, **80**, 5851–5858.
40 S. Stapf and R. Kimmich, Translational versus rotational molecular dynamics in plastic crystals studied by NMR relaxometry and diffusometry, *Mol. Phys.*, 1997, **92**, 1051–1060.
41 O. Yamamuro, H. Yamasaki, Y. Madokoro, I. Tsukushi and T. Matsuo, Calorimetric and neutron scattering studies of plastically crystalline cyclooctanol, *J. Phys.: Condens. Matter*, 2003, **15**, 5439–5450.
42 E. Novak, N. Jalarvo, S. Gupta, K. Hong, S. Förster, T. Egami and M. Ohl, Dynamics in the Plastic Crystalline Phases of Cyclohexanol and Cyclooctanol Studied by Quasielastic Neutron Scattering, *J. Phys. Chem. B*, 2018, **122**, 6296–6304.
43 H. Wagner and R. Richert, Equilibrium and non-equilibrium type β-relaxations: D-sorbitol *versus* *o*-terphenyl, *J. Phys. Chem. B*, 1999, **103**, 4071–4077.
44 S. Lansab, P. Münzner, H. Zimmermann and R. Böhmer, Deuteron nuclear magnetic resonance and dielectric studies of molecular reorientation and charge transport in succinonitrile-glutaronitrile supercooled plastic crystals, *J. Non-Cryst. Solids X*, 2022, **14**, 100097.
45 P. Steeman and J. van Turnhout, Fine Structure in the Parameters of Dielectric and Viscoelastic Relaxations, *Macromolecules*, 1994, **27**, 5421–5427.
46 M. Wübbenhorst and J. van Turnhout, Analysis of complex dielectric spectra. I. One dimensional derivative techniques and three-dimensional modelling, *J. Non-Cryst. Solids*, 2002, **305**, 40–49.
47 N. Bloembergen, E. M. Purcell and R. V. Pound, Relaxation Effects in Nuclear Magnetic Resonance Absorption, *Phys. Rev.*, 1948, **73**, 679–712.
48 R. K. Kadiyala and C. A. Angell, Separation of nucleation from crystallization kinetics by two step calorimetry experiments, *Colloids Surf.*, 1984, **11**, 341–351.

49 D. Farhat, *Etude d'électrolytes à base de dinitriles aliphatiques pour des batteries Li-ion*, PhD Dissertation, Université de Tours, 2017, **https://www.theses.fr/2017TOUR4035/document**.
50 T. R. Kartha and B. S. Mallik, Molecular Dynamics and Emerging Network Graphs of Interactions in Dinitrile-Based Li-Ion Battery Electrolytes, *J. Phys. Chem. B*, 2021, **125**, 7231–7240.
51 C. T. Moynihan, N. Balitactac, L. Boone and T. A. Litovitz, Comparison of Shear and Conductivity Relaxation Times for Concentrated Lithium Chloride Solutions, *J. Chem. Phys.*, 1971, **55**, 3013–3019.
52 J. C. Dyre, On the mechanism of glass ionic conductivity, *J. Non-Cryst. Solids*, 1986, **88**, 271–280.
53 P. Sippel, S. Krohns, D. Reuter, P. Lunkenheimer and A. Loidl, Importance of reorientational dynamics for the charge transport in ionic liquids, *Phys. Rev. E*, 2018, **98**, 052605.
54 I. M. Hodge, K. L. Ngai and C. T. Moynihan, Comments on the electric modulus function, *J. Non-Cryst. Solids*, 2005, **351**, 104–115.
55 K. L. Ngai and A. K. Rizos, Parameterless explanation of the non-Arrhenius conductivity in glassy fast ionic conductors, *Phys. Rev. Lett.*, 1996, **76**, 1296–1299.
56 F. Mizuno, J.-P. Belieres, N. Kuwata, A. Pradel, M. Ribes and C. A. Angell, Highly decoupled ionic and protonic solid electrolyte systems, in relation to other relaxing systems and their energy landscapes, *J. Non-Cryst. Solids*, 2006, **352**, 5147–5155.
57 M. Aniya and M. Ikeda, A Model for Non-Arrhenius Ionic Conductivity, *Nanomaterials*, 2019, **9**, 911.
58 C. Bischoff, K. Schuller, S. P. Beckman and S. W. Martin, Non-Arrhenius Ionic Conductivities in Glasses due to a Distribution of Activation Energies, *Phys. Rev. Lett.*, 2012, **109**, 075901.
59 G. P. Johari and O. Andersson, On the nonlinear variation of dc conductivity with dielectric relaxation time, *J. Chem. Phys.*, 2006, **125**, 124501.
60 C. M. Roland, S. H. Bielowka, M. Paluch and R. Casalini, Supercooled dynamics of glass-forming liquids and polymers under hydrostatic pressure, *Rep. Prog. Phys.*, 2005, **68**, 1405–1478.
61 D. Reuter, P. Münzner, C. Gainaru, P. Lunkenheimer, A. Loidl and R. Böhmer, Translational and reorientational dynamics in deep eutectic solvents, *J. Chem. Phys.*, 2021, **154**, 154501.
62 A. Schulz, P. Lunkenheimer and A. Loidl, Lithium-salt-based deep eutectic solvents: Importance of glass formation and rotation-translation coupling for the ionic charge transport, *J. Chem. Phys.*, 2021, **155**, 044503.
63 A. Schulz, K. Moch, Y. Hinz, P. Lunkenheimer and R. Böhmer, Translational and reorientational dynamics in carboxylic acid-based deep eutectic solvents, *J. Chem. Phys.*, 2024, **160**, 074503.
64 H. J. V. Tyrrell and K. R. Harris, *Diffusion in Liquids: a theoretical and experimental study*, Butterworths, London, 1984.
65 I. Chang and H. Sillescu, Heterogeneity at the Glass Transition: Translational and Rotational Self-Diffusion, *J. Phys. Chem. B*, 1997, **101**, 8794–8801.
66 F. Qi, K. U. Schug, A. Döß, S. Dupont, R. Böhmer, H. Sillescu, H. Kolshorn and H. Zimmermann, Structural relaxation of the fragile glass-former propylene carbonate studied by nuclear magnetic resonance, *J. Chem. Phys.*, 2000, **112**, 9455–9462.
67 R. Meier, E. Schneider and E. A. Rössler, Change of translational-rotational coupling in liquids revealed by field-cycling ^{1}H NMR, *J. Chem. Phys.*, 2015, **142**, 034503.
68 J. T. Edward, Molecular Volumes and Stokes-Einstein Equation, *J. Chem. Educ.*, 1970, **47**, 261–270.
69 M. J. Lizak, R. C. Keller, M. S. Coffey, M. S. Conradi and W. Bunnelle, Rotation and pseudorotation in solid cyclooctane, *J. Phys. Chem.*, 1990, **94**, 992–994.
70 C. A. Stortz, Conformational pathways of simple six-membered rings, *J. Phys. Org. Chem.*, 2010, **23**, 1173–1186.
71 I. Kishimoto, J. J. Pinvidic, T. Matsuo and H. Suga, Phase Transition and Glass Transitions in Isocyanocyclohexane Studied by a Polaro-Calorimeter, *Proc. Jpn. Acad., Ser. B*, 1991, **67**, 66–71.
72 F. S. Howell, R. A. Bose, P. B. Macedo and C. T. Moynihan, Electrical Relaxation in a Glass-Forming Molten Salt, *J. Phys. Chem.*, 1974, **78**, 639–648.
73 A. Pimenov, P. Lunkenheimer, M. Nicklas, R. Böhmer, A. Loidl and C. A. Angell, Ionic transport and heat capacity of glass-forming metal-nitrate mixtures, *J. Non-Cryst. Solids*, 1997, **220**, 83–101.
74 B. Roling, Scaling properties of the conductivity spectra of glasses and supercooled melts, *Solid State Ionics*, 1998, **105**, 185–193.
75 J. Habasaki, C. León and K. L. Ngai, *Dynamics of Glassy, Crystalline and Liquid Ionic Conductors: Experiments, Theories, Simulations*, Springer, Switzerland, 2017.
76 J. Beerwerth, S. P. Bierwirth, J. Adam, C. Gainaru and R. Böhmer, Local and global dynamics of the viscous ion conductors $2Ca(NO_3)_2$–$3KNO_3$ and $2Ca(NO_3)_2$–$3RbNO_3$ probed by 87Rb nuclear magnetic resonance and shear rheology, *J. Chem. Phys.*, 2019, **150**, 194503.
77 T. Yamaguchi and S. Koda, Dielectric and shear relaxations of ionic liquid composed of symmetric ions, *J. Chem. Phys.*, 2014, **141**, 144503.